Sensing Wood Moisture in Heritage and Wooden Buildings: a New Sensing Unit with an Integrated LoRa-based Monitoring System

Mohamed Saban*,**, Silvia Casans-Berga*, Rafael García-Gil*, A. Edith Navarro-Antón*, Otman Aghzout**, and Alfredo Rosado-Muñoz*

***Abstract*—The rapid development of LoRa and LoRaWan received a wide interest in research in order to understand the performance of this technologies for various IoT applications. In this article, we propose an IoT system for smart buildings based on LoRa and LoRaWan. The main aim of this system is monitoring the moisture of wood in buildings; specifically in cultural heritage buildings; using wireless sensor nodes that are digitally controlled with low-power consumption. A new moisture sensor that relies on a novel resistance measurement method was developed and tested, including a new printed circuit board (PCB). This sensor comprise a LoRa communication module in order to be used as the end-node of the proposed system. A cloud-based monitoring application was developed to provide remote visualization and control for all LoRa sensor nodes. The proposed system is scalable and represents a practical solution for early detection of wood moisture due to heavy rain, leaks, etc. The path loss was evaluated, the results showed that the proposed LoRa system can be applied for preservation of heritage buildings despite the attenuation due to thick walls and complex architectural structures.**

***Index Terms*—cloud server, IoT, Moisture Content, wood resistance measurement, wood polarization effect, LoRa, LoRaWan, Wireless monitoring**

I. Introduction

CULTURAL heritage has an inestimable value around the world. The protection of cultural heritage such as historical buildings is a major challenge due to its exposure to significant natural and man-made risks. As timber is a commonly used construction material since ages, monitoring its Moisture Content (MC) is crucial to forecast and prevent damages, especially for old buildings where timber has been exposed to environmental changing conditions along time. The MC is an important value as it affects the weight and the strength of wood [1]–[4]. A high MC value above saturation point of the fiber (above 30% MC) increases the risk of biological attacks and leads to wood deterioration [5].

Structural timber is usually located in hidden and inaccessible locations in a building, making monitoring difficult. In this case, a Wireless Sensor Network (WSN) represents a feasible solution. They are used for diverse monitoring applications including smart agriculture [6], fire monitoring [7], water monitoring [8], building structural monitoring [9], indoor air quality monitoring [10]. In most cases, WSN have stringent power requirements to keep continuous monitoring for extended periods of time. Hence, the management of the power source must be taking into account for sensors in a WSN [11].

Applications based on Internet of Things (IoT) offer many solutions to facilitate monitoring and it can be used to prevent potential risks such as moisture in case of wooden buildings. The IoT is currently evolved in multiple domestic and industrial systems, offering many application domains and communication protocols [12], [13]. The International Data Corporation (IDC) expects that the number of IoT connected devices will reach 41.6 billion by 2025 [14]. These devices are connected to cloud servers processing the collected data and allowing the users to remotely control and monitor them through web and mobile applications.

In the literature, many works describe the use of IoT systems for cultural heritage monitoring. The authors in [15] shows the role of IoT to support cultural heritage inventory. In [16], a smart archive box for museum artifact monitoring using battery-less temperature and humidity sensing was proposed. In [17], the authors combine an integrated informative system for maintenance and preservation of artistic assets. The authors in [18] present a wireless sensor platform for cultural heritage monitoring and modeling system. Besides, several IoT-based monitoring approaches for cultural heritage sites were proposed in [19]–[22].

Currently, multiple communication technologies to support the different types of IoT systems exist. The selection criteria is based on the data rate, the coverage area, and power consumption. Low-Power Wide-Area Networks (LPWAN) are characterised by broad coverage, low power consumption and good scalability. In this context, LoRa is an adequate air interface technology for LPWAN [23] that became very popular in the past few years. It allows the construction of public networks for several applications, which makes it a key part in the development of IoT [24]. LoRa can handle a large number of sensor nodes with a coverage in the range of kilometres (depending on the environmental obstacles) while requiring low power during transmission.

This paper illustrates a Smart Building application using LoRa and LoRaWan technologies. A new timber MC sensor able to form a WSN based on LoRa was developed and tested. This sensor stores remotely the measured data in a cloud server. A web-based platform is built to provide a user interface accessible through a web browser, which allows

Manuscript received XXXXX, 2022. The authors are with the Department of Electronic Engineering. University of Valencia. 46100 Burjassot. Spain*, and also with the Université Abdelmalek Essaadi, ENSA Tetouan, Morocco**. (e-mail: mohamed.saban@uv.es).

the remote control of the network devices (sensor nodes and gateways, monitoring and analysing the received data, as well as general management options (users, permissions, etc.) under multiple screen sizes and devices with different operating systems.

This document is organized as follows: Section II describes a brief review of LoRa and LoRaWan. Section III describes the developed moisture sensor. Section IV represents all different tests performed and types of wood analyzed in order to verify the sensor accuracy and the WSN functionality in a real scenario of a historical building. Lastly, Section VI describes the web management application, and Section VII concludes the paper.

II. LoRa and LoRaWan Overview

LoRa is a proprietary Chirp Spread Spectrum (CSS) modulation technique patented by Semtech [25]. LoRa affords high sensitivity for the receiver and increases the robustness against noise [26]. The modulation technique utilizes six orthogonal Spreading Factors (SF) ranging from 7 to 12 with a trade-off between higher data rate and long range, or power. A lower SF results in a higher receiver sensitivity [27] but more power is required, and vice-versa. In Europe, LoRa uses the 863-870 MHz frequency band. It can operate in two sub-bands, one at 868 MHz offering 3 LoRa channels of 125 kHz each, and one at 867 MHz offering 5 LoRa channels of 125 kHz [28]. Through regulation, a duty cycle limitation (1%) is applied as the method of channel access and to avoid collision. The duty cycle represents the delay between the successive frame sent by the device using the same channel.

LoRaWAN is a Medium Access Control (MAC) layer open protocol proposed by LoRa Alliance and provides the mechanism to enable the communication between LoRa devices using LoRaWAN gateways. LoRaWAN has a star topology architecture: peer to peer connection is not possible between end devices, they can only communicate with the receiver (LoRa gateway). However, multiple gateways can be connected to a central LoRaWan cloud server. Thus, a complete WSN based on LoRa consists of three main components as shown in Fig. 1: LoRa end-nodes, LoRaWAN gateways and a cloud server [29].

The LoRa end-nodes communicate with the LoRaWAN gateways through LoRa physical layer. The gateway relay packets of data transparently between the LoRa end-nodes and the cloud server. The connection between the cloud server and the gateway is established over IP-backhaul with a high throughput (wired or via cellular network). Each LoRa end-node can communicate with different gateways, they are not associated with a specific gateway, thus, a packet can be delivered to the cloud server through multiple gateways [30]. The cloud server selects a reliable packet in case of receiving the same packet from multiple gateways.

The architecture proposed by LoRa/LoRaWAN fits the requirements in this application since end-node MC sensors send data information with a high period of time (very low bandwidth required). In addition, a low power is required for the sensors as they will be located in inaccessible locations and then, long battery life is a must. Thus, nodes can be placed in selected locations in a building to continuously monitor the timber MC, being able to provide early detection in case of high MC due to leakages or timber deterioration, in general.

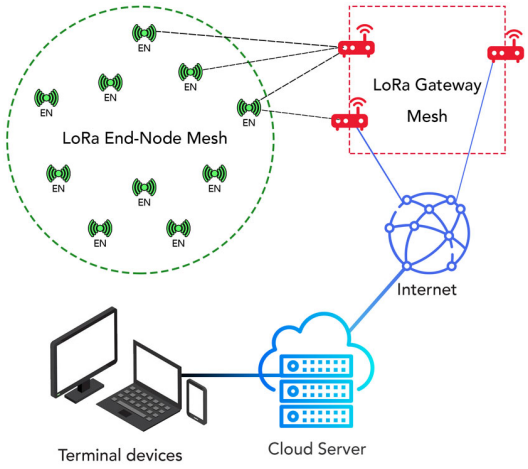

Fig. 1. LoRa/LoRaWan Mesh Networking.

III. LoRa End-node MC sensor

This section is divided into two parts. The first part will describe the structure and functionality of the end-node sensor developed and the second part describes the conditioning circuit used to measure the MC in wood.

A. Description of the new end-node sensor

A new electronic board was designed for the LoRa MC end-node sensor. It integrates the sensing part and the LoRa communication in a single board to optimize size and power. The components of the moisture sensor are presented in Fig. 2. It consists of four blocks, namely:

- Sensing unit: contains the AC measurement circuit to measure MC in wood, and a temperature sensor. This section provides the proper values able to be read by the processing unit.
- Processing unit: contains a programmable microcontroller where specific firmware was developed to control the sensing and LoRa transmitting and receiving operations. The firmware also includes power management to optimize power consumption.
- Communication unit: performs the data exchange between the sensor node and the LoRa gateway using the LoRa standard communication protocol.
- Power unit: The board will be powered using two standard 1.5 V AAA batteries. This power section regulates a constant 3.3 V output to supply the processing and communication units. It also generates a symmetrical ± 15 V_{DC} for the sensing unit.

In this board, the processing and communication units are integrated in the commercial module WiMOD iM881-XL from IMST [31]. It provides ultra-long range spread spectrum

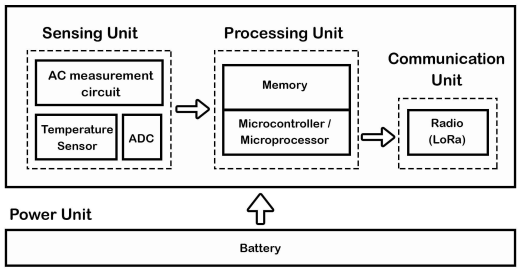

Fig. 2. Components of the LoRa end-node moisture wireless sensor.

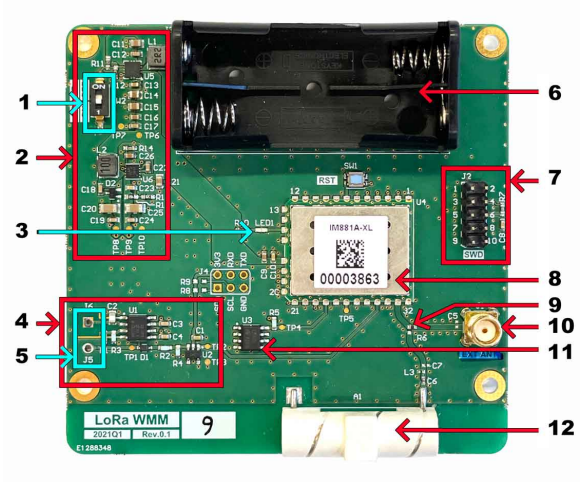

Fig. 3. LoRa end-node Moisture Sensor board.

communication and high interference immunity. The iM881A-XL operates in the 868 MHz Industrial, Scientific, and Medical (ISM) band with a powering voltage from 1.8 V to 3.6 V, and uses Semtech's patented LoRa modulation technique which combines spread spectrum modulation and forward error correction techniques. The iM881A-XL is directly solderable as an SMD component and it is pre-certified according to the European guideline EN 300 220 [31]. This LoRa module is equipped with a programmable STM32L081 microcontroller (MCU) optimized for battery driven applications. The specific firmware application will reside in this unit. The iM881-XL main features are the following:

- Operating voltage: 1.8 V to 3.6 V.
- Operating frequency: ISM 868 MHz.
- Operating temperature range: -40 °C to +85 °C.
- Receiving current: 11.2 mA.
- Transmitting current: 25 mA to 38 mA.
- Low Power mode current: 1.4 μA.
- Sensitivity: -138 dBm.
- MCU operation frequency: 32 MHz.

Fig. 3 describes the resulting board, with 81 × 83 mm in size. The components of the board are listed below:

1) Sliding switch to power up the device.
2) Power supply regulation components.
3) LED to inform about different operation according to blinking codes.
4) MC measurement circuit.
5) Wood probes connector.
6) Battery holder type AAA.
7) Programming connector for firmware update and debugging.
8) Wireless LoRa Module.
9) Switch between integrated and external antennas.
10) External SMA antenna connector.
11) Temperature sensor LM335DT.
12) Integrated PCB Antenna W3136.

As described above, the board contains two different antenna connections: internal and external. This possibility allows to reduce size with internal connection but also can be used with an external antenna in case that long range communication is required. An internal switch located in the board for this purpose. The board shown in Fig. 3 is selected to operate with the external antenna.

B. Moisture Content Measurement Circuit

Direct and indirect methods can be used to measure MC in wood [4], [32]. Typically, when it comes to timber already fixed in buildings, indirect methods are applied. The indirect methods are based on the measurement of a physical property of wood that depends on its MC (e.g. electrical resistance for the resistive method [33], [34], dielectric constant for the capacitive method [1], [35], microwave methods [1] or sorption capacity methods [36]).

The resistive method is a common indirect method to calculate the MC in wood [32]–[34]. By creating an electric current path between a pair of electrodes rammed into the wood, its electrical resistance R is measured. The wood MC is directly related to its resistivity (ρ), which is measured by its electrical resistance R defined in Equation 1.

$$R = \frac{\rho L}{A} \tag{1}$$

Where (ρ) represents the resistivity, L the distance separating the two electrodes, and A the current area transversal section. Hence, R depends on the geometry of the wood piece, the wood species, and the position of the rammed electrodes, among others [37], [38].

The current applied to the electrodes can be both Direct Current (DC) [33], [34] or Alternating Current (AC) [39]–[41]. Polarization effects may occur when applying DC [38], [40], thus an AC method is preferred to minimise the initial transient response when measuring the electrical resistance R.

The AC method used in this work is based on the relaxation oscillator shown in Fig. 4 [39]. With this oscillator, the wood automatically sets the oscillation frequency f of the applied AC depending on the wood electrical resistance (R_w in Fig. 4). The capacitor C_2 is charged/discharged through V_0 voltage and R_w, generating a square signal between +V_{sat} and -V_{sat} when V_t reaches the threshold values V_{tmax} and V_{tmin}, respectively (see Fig. 4) as described in Equation 2.

$$\begin{aligned} V_{tmax} &= \frac{R_1}{R_1+R_3} V_{sat} \\ V_{tmin} &= -\frac{R_1}{R_1+R_3} V_{sat} \end{aligned} \tag{2}$$

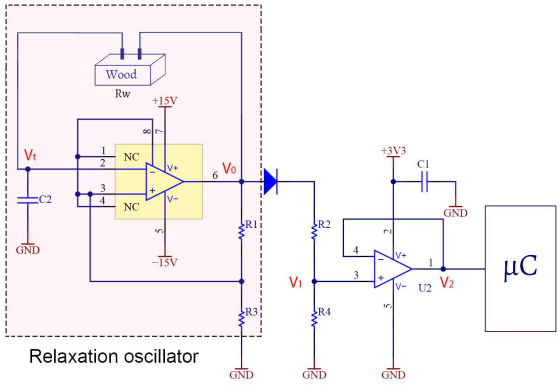

Fig. 4. Electronic circuit for MC calculation using a resistive method based on AC.

Assuming that saturation voltages +V_{sat} and -V_{sat} of the operational amplifier U_1 are symmetrical, the oscillation time period T linearly depends on R_w as Equation 3 describes.

$$T = 2\ln(\frac{R_1 + 2R_3}{R_1})R_w C_2 \tag{3}$$

Thus, the wood resistance R_w can be indirectly obtained by measuring the period T. This period is measured and converted into wood resistance by the microcontroller (Fig. 2), with the corresponding voltage adjustment as seen in Fig. 4 (V_0, V_1, V_2) [39]. The simplified flow diagram of the developed program to compute the period T for the STM32L081 microcontroller is shown in Fig. 5.

The ±15 V power-supply required by operational amplifier U_1 in Fig. 4 is generated by the low-input boost converter TPS61093DSK. This regulator includes an enable pin which permits the microcontroller to activate the circuit only when measuring the wood resistance, thus saving battery energy. After taking the measurements, the device send the average value to the gateway and enter in a sleep mode for a period of time that can be configured in the platform by the user.

The Sensing Unit (Fig. 2) also includes the LM335DT temperature sensor since the MC value conversion from R_w measurement depend on temperature [42]–[44]. The LM335DT has an accuracy of ±1 °C.

IV. Experimental Tests and Results

Two different analyses were carried out. In the first analysis, the MC LoRa end-node was characterized by means of a calibration process at a stable temperature of 25°C. From this calibration, the accuracy of the resistance measurement is obtained. Then, a thermal analysis is included and its effect on accuracy is considered. Finally, the correlation between the wood resistance and the MC is given. In the second analysis, the LoRa communication is analyzed to obtain the real 'in the field' capabilities of the developed MC LoRa end-node: range, data transmission, and communication link stability between end-nodes and the LoRa gateway. For an adequate study on the capabilities of the proposed MC monitoring system, a real scenario was used.

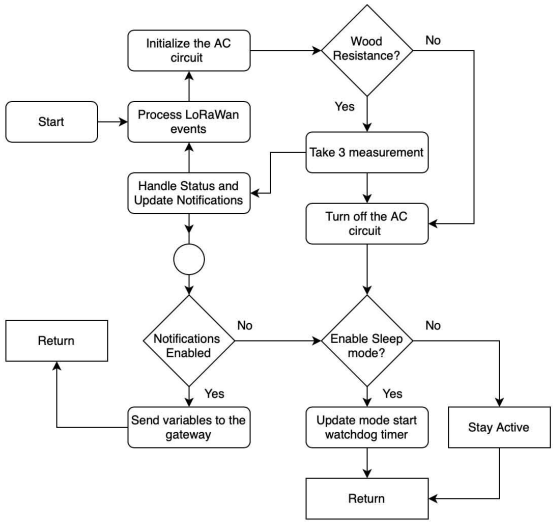

Fig. 5. Simplified diagram flow for the configuration of the moisture device.

A. MC Measurement Circuit: Functional Test

The calibration of the MC LoRa end-node was performed in a laboratory at a stable temperature of 25 °C. The calibration process consists of measuring the oscillation period T of circuit in Fig. 4 for different R_w of known value. For this process, a calibrated resistance decade box (IET model VRS-100) was used, with resistance values between 10 $M\Omega$ and 10 $G\Omega$ (typical wood resistance values when wood changes from humid to very dry). As a linear correlation between the measured period T and R_w according to equation (3) exists, a linear fit has been considered. Equation 4 allows estimating the resistance value R_w , where K= 322.9 Ω/s.

$$R_w = K \cdot T \tag{4}$$

Table I shows the obtained results for the three analysed PCBs, where R_d represents the resistance values fixed by the calibrated decade box, expressed in $M\Omega$, T is the period obtained using the measurement circuit, R_w represents the resistance estimated by the MCU using the obtained period T and ϵ_r describes the relative error.

Results show that an error lower than 2 % is obtained for the R_w measurement, this means that the resistance value can be accurately obtained from the T period measured by the sensing circuit in the MC LoRa end-node.

According to Samuelson's equation [42], the wood MC is related with its resistance R_w through the expression given in Equation 5 where MC is given in %, R_w in $M\Omega$; a and b are model coefficients which values depend on the wood species [43], [44].

$$MC = \frac{log[log(R_w) + 1] - b}{a} \tag{5}$$

Using Equation 5, the MC relative error is given by Equation 6.

$$\epsilon_{MC} = \frac{\epsilon_r}{ln10^2 \times [log(R_w) + 1] \times [log(log(R_w) + 1) - b]} \tag{6}$$

TABLE I
ACCURACY ANALYSIS FOR RESISTANCE MEASUREMENT: CALIBRATED RESISTANCE VALUE R_d, OBTAINED PERIOD T, MEASURED RESISTANCE R_w USING EQUATION 4, AND THE RESISTANCE RELATIVE ERROR ϵ_r FOR THREE DIFFERENT MC LORA END-NODE BOARDS (PCB#1,2,3).

PCB	R_d (MΩ)	T(s)	R_w (MΩ)	$\epsilon_r(\%)$
1	10.000028	0.0309	9.935975	0.2
	100.001730	0.3046	98.463497	1.6
	1000.183000	3.0620	995.092578	1.1
	10016.717000	30.8620	10083.190000	0.5
2	10.000028	0.0311	10.042190	0.4
	100.001730	0.3101	100.115145	0.1
	1000.183000	3.0913	998.180770	0.2
	10016.717000	31.2502	10090.689601	0.7
3	10.000028	0.0309	9.990526	0.1
	100.001730	0.3090	99.759955	0.3
	1000.183000	3.1121	1004.906780	0.5
	10016.717000	30.9608	9997.245550	0.2

From Equation 6, it can be interpreted that $\epsilon_r < 2$ % in R_w typically implies $\epsilon_{MC} < 0.2$ % in the MC value (slightly dependent on the wood species).

B. Thermal Characterization of the Sensing Unit.

The MC LoRa end-node developed include a sensing unit that works with very low-level currents (pA). These currents sometimes are comparable with the leakage currents involved in the circuitry components at high temperatures [45], [46], making the measurement error unacceptable. As the MC LoRa end-node is going to be exposed to outdoor locations and sometimes exposed to the elements, it is really important to get its thermal characterization.

To evaluate its behavior at different temperatures, a climate chamber was used. The temperature was set from 25 °C with increments of 5 °C until 50 °C. During this test, the calibrated resistance decade box was used, set at four different resistance values.

The experimental results obtained during this thermal characterization showed a repetitive behaviour for each temperature, according to Equation 4.

The maximum relative error obtained was lower than 3 % implying an error lower than 0.3 % in the MC value. This fact means that the MC LoRa end-node developed can be used in a wide temperature range without any thermal compensation.

C. MC measurement in different wood species.

After verifying the accuracy under calibrated resistance values, the MC LoRa end-node was tested in wood using Equation 5 to obtain the corresponding MC. three different wood species were selected: oregon pine (Pseudotsuga Menziesii), european ash (Fraxinus Excelsior), and chestnut tree (Castanea Sativa). Their corresponding a and b parameters from Equation 5 were obtained [43], [44], [47], [48] and listed in Table II. The dimensions of each timber piece were $90 \times 35 \times 45$ mm. Two 0.7 mm diameter iron nails rammed in the center of each timber piece were used as electrodes (Fig. 6 (a)), inserted 10 mm deep with a separation of 20 mm. The test was performed during three days with small environmental conditions variations: temperature between 23 °C and 27 °C, and relative humidity between 55 % and 63 %. Each MC LoRa end-node was sending 10 measurement per hour.

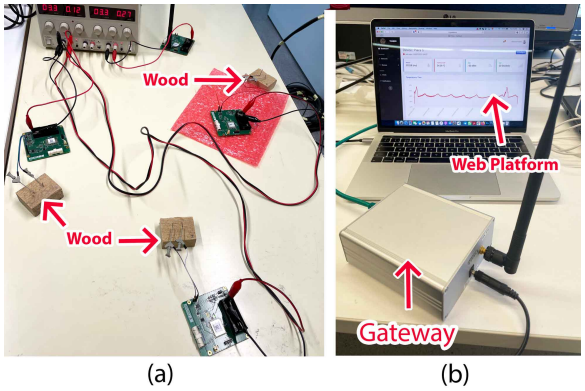

Fig. 6. Test bench used for the circuit characterization. (a) Resistance measurement in three timber pieces from different species of wood (Pine: seudotsuga Menziesii, Ash: Fraxinus Excelsior, Chestnut: Castanea Sativa. Each timber piece was measured by an MC LoRa end-node board, (b) LoRaWan gateway and developed web platform.

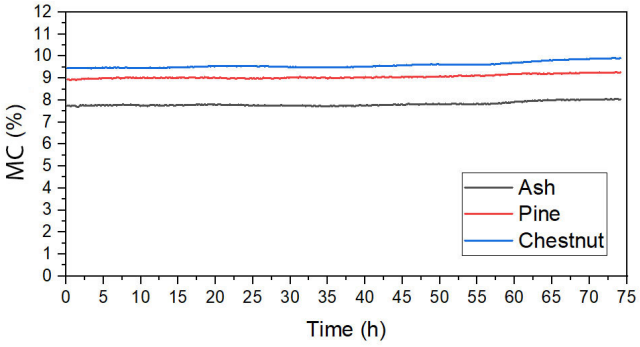

Fig. 7. MC measured during 3 days under ambient conditions for pine, ash and chestnut wood species.

TABLE II
PARAMETERS a AND b OF EQUATION 5 ASSOCIATED TO EACH WOOD SPECIES.

Wood species	a	b
Oregon pine (Pseudotsuga Menziesii)	-0.045000	1.14700
European ash (Fraxinus Excelsior)	-0.051567	1.13545
Chestnut tree (Castanea Sativa)	-0.039347	1.02940

A web platform (Fig. 6 (b)) was developed for data storage, visualization, and analysis. In this web, equation 5 and coefficients a and b for different wood species are programmed to obtain the MC value. The resultant MC measurements over the time are shown in Fig. 7, giving values lower than 10% as expected since the wood was stored in the laboratory during two years.

V. PATH-LOSS EVALUATION IN LORA COMMUNICATION

As LoRaWan aims at long distances, we can find many studies that focused on testing LoRa and LoRaWan in outdoor

environments [49]–[51]. The performance of LoRa communication between end-nodes and the gateway in indoor environments also received much research interest; several works were presented to study the propagation of LoRa inside buildings [52]–[54]. The work presented in this paper is developed to be used by maintenance services in timber-based buildings to anticipate damages in case of water leakage or other wood deterioration. Old historical building are composed of multiple areas connected, both indoor (e.g. rooms) and outdoor (e.g. yards). Then, indoor and outdoor experimental test were carried out to account for multiple cases of end-nodes location. Hereafter, the first experiment was conducted in an outdoor urban environment and the second test was done inside a historical building.

In this work, The Things Network (TTN) is used for LoRaWan communication. TTN is an initiative to build an open source worldwide infrastructure based on LoRaWan standards, it enables low power end-nodes to leverage existing gateways to connect to an open-source network to facilitate the public use of IoT devices [55]. TTN is a decentralized and collaborative network, containing thousands of LoRaWan gateways around the globe. It offers a web interface where the users can add their devices and control the collected data, as well as adding new gateways to expand the network in a collaborative way.

The gateway used in this paper is 'WiMOD LoRa Lite Gateway' from IMST, this gateway basically consists of a Raspberry Pi and an iC880A connector. The configuration used for the end-node devices is listed bellow:

1) LoRa Class: Class A
2) Frequency: 867.1–868.5 Mhz
3) Bandwidth size: 125 kHz
4) Spreading Factor (SF): 7
5) Coding Rate: fixed = 4/5
6) Transmitting Power: +14 dB
7) Transmitting Antenna gain: +2 dB
8) Receiving Antenna gain: +2 dB

In the following experiments, the Large-Scale Fading (LSF) is characterized by its Path Loss parameter (PL). Modelling of signal propagation is an important topic in some applications, such as Wireless Sensor Network location system. The ratio between the received power P_r and the transmitted power P_t in a free space environment is given by the Friis law (Equation 7).

$$\frac{P_r}{P_t} = G_t G_r (\frac{\lambda}{4\pi d})^2 \tag{7}$$

where G_t and G_r are the gains of the transmitter and the receiver, respectively; λ is the wave length, and d is the distance between the transmitter and the receiver.

For non-free space environment, a path loss exponent γ and a reference distance are introduced. Then, Equation 7 becomes Equation 8.

$$\frac{P_r}{P_t} = G_t G_r (\frac{\lambda}{4\pi})^2 \times \frac{1}{d_0^{\gamma}} \times (\frac{d_0}{d})^{\gamma} \tag{8}$$

Using the first-order fit [56], PL can be estimated by modelling the experimental PL. the Estimated Path Loss (EPL) can be obtained by Equation 9.

$$EPL = PL_0 + 10 \times \gamma \times log_{10}(\frac{d}{d_0}) \tag{9}$$

where PL_0 is the PL intercept at the reference distance d_0, determined by measurements for microcellular systems, normally it varies between 1 m and 100 m. In this paper, we consider d_0 = 1 m, γ represents the PL exponent that indicates the nature of the propagation environment and it can be estimated from the measurement results. In the literature, we can find some algorithms that help to estimate the exponent value such as the algorithm presented by Wojcicki [57]. Typically, in free-space environment γ= 2, in urban environment γ varies between 2.7 and 3.5, whereas in building environments γ varies between 1.6 and 6 depending on the structure of the building, the material used for the construction, and the obstacles [58].

Due to shadow fading deviation, there is a difference between the path loss PL and the estimated path loss EPL as described in Equation 10.

$$\sigma_{SF} = std(PLEPL) \tag{10}$$

The path loss (PL) has been evaluated in outdoor and indoor environments on the basis of the measured RSSI and signal-to-noise ratio (SNR) using Equation 11 [59], where P_{Tx} is the transmission power G_{Tx} and G_{Rx} are the gains of the transmitting and receiving antennas, respectively.

$$PL = P_{Tx} + G_{Tx} + G_{Rx} + 10 \times \log_{10}(1 + \frac{1}{SNR}) - RSSI \tag{11}$$

The percentage of the received packets (RPP) was calculated in each location as described in Equation 12, where NACK denotes the number of packets with 'Acknowledgement' signal received, and NAP denotes the number of all transmitted packets.

$$RPP[\%] = 100 \times \frac{NACK}{NAP} \tag{12}$$

In this test, measurement points with RPP below 50% are ignored. The collected data with the superimposed PL measurements and the model parameters in Equation 9 compared to the free-space path loss FSPL. hlthe previous sentence does not have sense for me

A. Urban environment performance test for LoRa communication

The first test was conducted in the center of Valencia city, Spain. As shown in Fig. 8 (b), the LoRa gateway receiver was placed on the roof of a 10-floor building with an altitude of 40 m, approximately. The gateway is powered and connected to the internet with an Ethernet cable.

Fig. 8 (a) is a screenshot from the TTN website, showing the active gateways at the time of the test. To avoid the interference with other LoRa gateways existing in the area, all the measurement points are situated in the south east to guarantee that

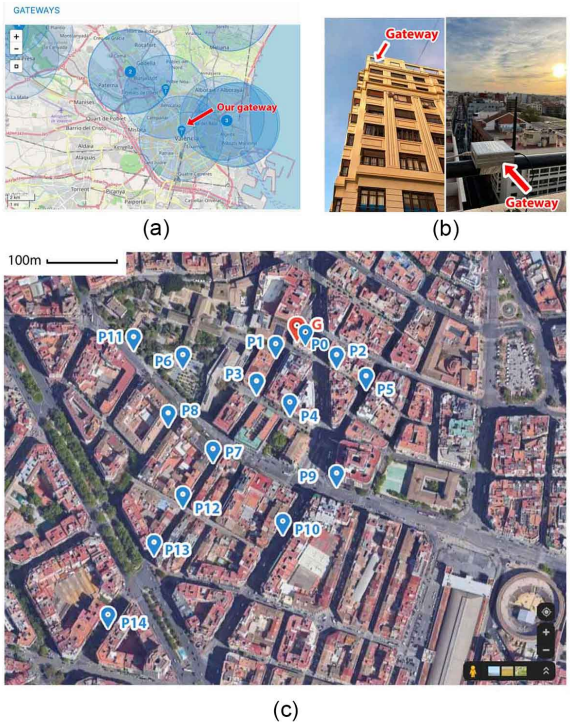

Fig. 8. Experimental setup for outdoor LoRa communication tests. (a): Screenshot from the TTN website showing the location of the active gateways in the test area. (b): LoRa gateway setup in a highly populated area. (c): P0 to P14 represent the measurement locations, G represent the gateway location and PR represent the reference position where the distance equals 1 meter.

the packets will be received by our gateway. The measurement points are described by letter (P) in Fig. 8 (c), the red point (G) refers to the gateway. From each location, 10 messages were sent containing the following information: transmitting time, end-node device EUI (identification number), base station EUI, encrypted and decrypted payload, frequency, data rate spreading factor and bandwidth, Signal to Noise Ratio (SNR) and Received Signal Strength (RSSI).

Table III represents the distance between the measurement locations and the LoRa gateway for each location.

TABLE III
PERCENTAGE OF RECEIVED PACKETS RPP FROM EACH MEASUREMENT POINT IN THE OUTDOOR LORA COMMUNICATION TEST

Point	Distance (m)	RPP (%)
PR	1	100
P0	5	100
P1	52	100
P2	72	100
P3	89	100
P4	117	90
P5	127	100
P6	160	90
P7	196	100
P8	202	100
P9	212	80
P10	265	60
P11	287	60
P12	290	70
P13	390	60
P14	503	60

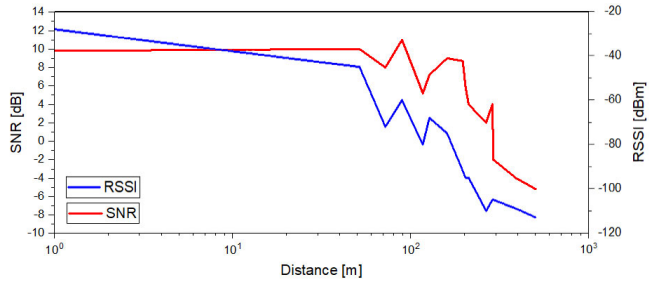

Fig. 9. LoRa communication parameter values in outdoor testing :Average RSSI[dBm] and Average SNR[dB] as a function of distance[m].

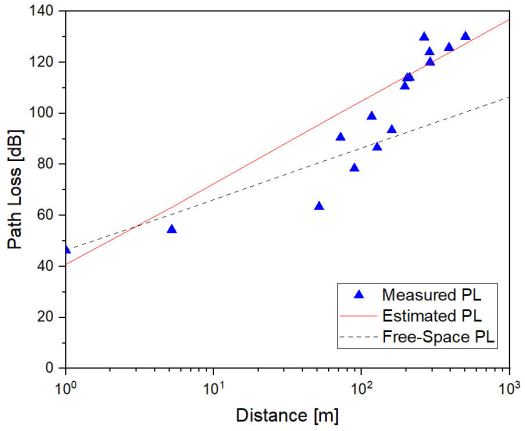

Fig. 10. Estimated and measured PL compared with the FS model in the urban environment.

Fig. 9 (a) and Fig. 9 (b) represents the average of RSSI and SNR measured in each measurement point respectively. The RSSI decreases as the distance increases. The first packet loss was at position P4 (117 m); however, at position P8 (202 m), all the packets arrived successfully. From position P7 the RSSI decreased under -90 dBm. Despite of that, SNR followed a similar trend: the SNR value stayed above 0 dB until P12 (290 m) and then it decreased to -5.2 dB at 500m.

TABLE IV
LOGNORMAL PL MODEL PARAMETERS IN THE OUTDOOR ENVIRONMENT.

EPL exponent (γ)	3.2
EPL intercept (PL(d_0))	40.82 dB
Standard deviation (σ_{SF})	5.6

The collected data with superimposed PL measurements calculated using Equation 11 are shown in Fig. 10. The EPL model parameters are described in Table IV. The results are compared with the free-space path loss FSPL model. The proposed model appears to be more valid as the distance increases. For distances shorter than 60m, the proposed model can be unstable mainly due to the shadowing effects, which affect propagation at smaller distances depending on the position of the end-node respecting the transmitter [59].

Fig. 11. Cultural Centre 'La Nau' where the LoRa monitoring system was installed.

(a) (b)

Fig. 12. Cultural center 'La Nau': (a) roof made of wood; (b) LoRa MC end-node sensor measuring values in the library section of the building.

B. Application in the field: Indoor test in a heritage building

The second experimental test was conducted in the Cultural Centre 'La Nau'. This historical building is the oldest emblematic facility for the University of Valencia, it was its head office since the foundation in the 15th century till the first half of the 20th century. The last important restoration was done in 1830 and it was declared Asset of Cultural interest in 1981 [60]. Fig. 11 depicts the external part of the building.

The constructed area of this building is 2900 m^2. As shown in Fig. 12 (a), most roofs of this building are made of wood, which makes the monitoring of wood conditions (mainly, moisture content) essential to avoid problems of water leaks and biological attacks.

The gateway was placed indoors, in a fixed position (P0) as described in Fig. 13, while the LoRA MC end-nodes were located in 15 different positions inside and outside the building. Then, the connectivity and the performance of the LoRa communication was tested. Firstly, to guarantee the validity of measurement results, a 100 MΩ $\pm 1\%$ resistor was used before connecting the real wood. Fig. 13 shows the plan of La Nau building and the location of the gateway and the different measurement points. Location P0 represents the gateway location in the ground floor, the red points represent

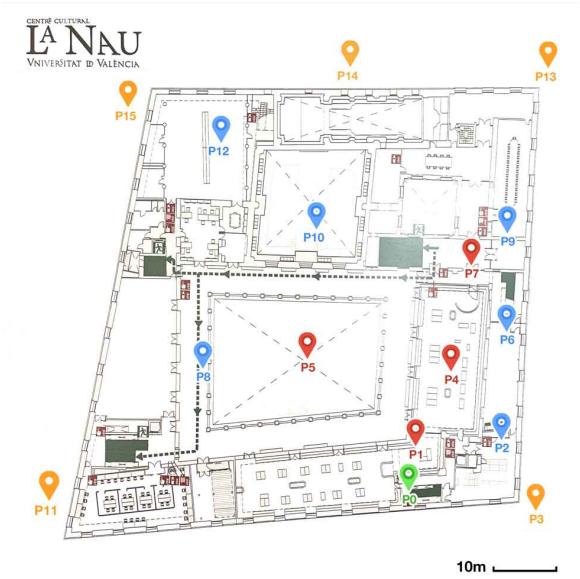

Fig. 13. Plan of the cultural Centre La Nau showing the position of the gateway (P0) and the location of different measurement points (P1 to P15) where the LoRa MC end-nodes were located. Red, blue and orange colors refer to the ground floor, first floor and second floor, respectively.

the measurement locations in the ground floor, the blue points are the measurement locations in the first floor while the orange points were in the ground floor, but situated outdoors.

A total of 10 messages were sent from each location. Each message contained the following information: transmitting time, end-node device EUI (identification number), base station EUI, encrypted and decrypted payload, frequency, data rate spreading factor and bandwidth, Signal to Noise Ratio (SNR) and Received Signal Strength (RSSI).

Fig. 14 represent the average RSSI and the average SNR measured in each measurement point. Typically, the range of LoRa SNR values range from -20 dB to +10 dB. A value closer to +10 dB means the receiver signal is less corrupted. In all the measurement points, the SNR value was positive, between 6.8 and 12 dB, whereas the RSSI did not follow a similar trend, it decreased to -101 dBm at P12 where the first packet loss occured, too. The big density of the materials used in this building prevents a good propagation of the LoRa radio waves when both end-node and gateway are indoor, having a big impact on RSSI.

In the previous outdoor test, the PL is predicted by a model that includes distance only. In the case of propagation inside a building, there are often obstructions between the gateway and the LoRa end-nodes, such as soft partitions, walls, and floors. Thus, in order to build a more accurate model, we need to consider the PL effects of these obstructions. In [61] and [62], this is achieved by including the attenuation factor of floor, soft partition, and walls in the prediction model. For simplicity, we include the attenuation factor of floors and walls assuming that any kind of obstacle that blocks totally or partially the direct path between the gateway and the end-node is labeled as a concrete wall. PL predicted by the attenuation factor model

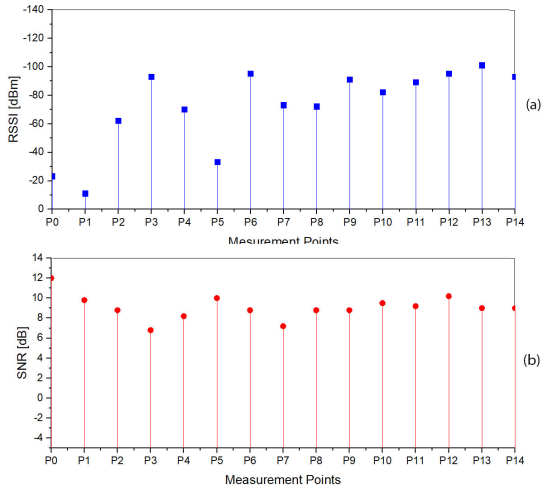

Fig. 14. LoRa communication analysis results in the heritage building: average SNR [dBm] and RSSI [dBm] measured in 15 points.

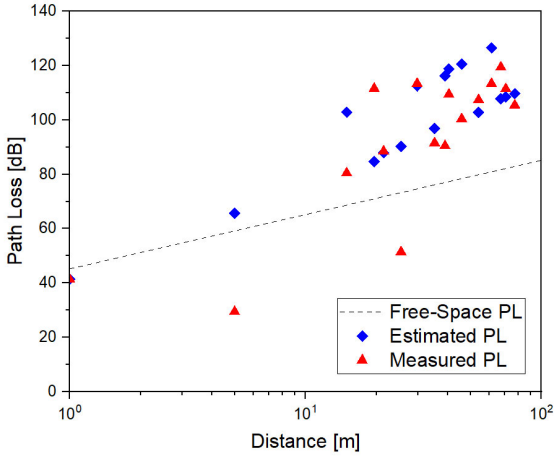

Fig. 15. LoRa communication analysis results in the heritage building: estimated and measured PL compared with the FS model.

can be estimated by Equation 13.

$$EPL = PL_0 + 10 \times \gamma \times log_{10}(\frac{d}{d_0}) + a \times AFF + b \times AFW \quad (13)$$

where AFF is the floor attenuation factor, AFW is the attenuation factor of a concrete wall, a is the number of floors and b represents the number of walls. A drive test was conducted to calculate the attenuation factors by calculating the PL where there is a wall separating the gateway and the end-node, and calculating again without wall, keeping the same separating distance. The same method was done in the case of the floor. The difference of PL is presented as the attenuation factor of each obstruction. After measuring the difference of PL in different locations of the building (different floors and walls), the final results are obtained by calculating the mean of these tests. Table V represents the distance separating the gateway from each measurement point including the number of walls and floors existing in the path. Table VI represents the EPL parameters of the indoor environment, the floor attenuation factor FAF and the walls attenuation factor WAF.

TABLE V
DISTANCE, NUMBER OF WALLS, NUMBER OF FLOORS AND RPP CORRESPONDING TO EACH MEASUREMENT POINT INSIDE THE HISTORICAL BUILDING

Point	Distance (m)	Walls	Floors	RPP (%)
P0	1.00	0	0	100
P1	4.90	1	0	100
P2	14.95	2	1	100
P3	19.55	1	0	100
P4	21.40	2	0	100
P5	25.40	2	0	100
P6	29.70	3	1	100
P7	35.25	3	0	100
P8	39.00	2	1	100
P9	40.50	3	1	100
P10	45.90	3	1	100
P11	54.10	3	0	100
P12	61.40	4	1	90
P13	67.25	4	0	100
P14	70.60	4	0	100
P15	77.00	4	0	100

TABLE VI
LOGNORMAL PL MODEL PARAMETERS IN THE INDOOR ENVIRONMENT.

EPL exponent (γ)	2.9
EPL intercept (PL(d_0))	41.34 dB
Standard deviation (σ_{SF})	6.7
FAF	20 dB
WAF	2 dB

The collected data with superimposed PL measurements calculated with Equation 11 and the estimated PL calculated with Equation 13 are shown in Fig. 15. The results are compared with the free-space path loss FSPL model. The figure shows that the measured PL at the gateway closely matches the proposed model. Hence, we can state that Equation 13 adequately represents the radio propagation of LoRa inside this building.

VI. TIMBERCARE: WEB MONITORING APPLICATION FOR MOISTURE CONTENT.

In this work, The Things Network (TTN) is also used for LoRaWan communication. TTN offers a web platform to read data from LoRa end-nodes and allows for simple and common data management. However, for specific purposes, a personalized platform is needed in order to customize the user control and analysis of data, as well as adding other functionalities not included in TTN web interface such as receiving alert messages via email or mobile phone, specific data visualization options and data retrieval, control user access control privileges, etc. Then, as TTN allows the integration of third party applications, this work developed a custom web interface called 'Timbercare' using the Model-View-Controller (MVC) based on the Laravel framework [63] and implemented with a MySQL database. The front-end of the web application is developed using Bootstrap framework, which provides a

responsive design to enable support for mobile devices, tablet and desktop interfaces (multiple screen sizes and touch panel friendly).

The Timbercare web application was hosted in a remote cloud server configured with LAMP (Linux, Apache, MySQL and PHP) software to complete the infrastructure of the whole system. Thus, the LoRa gateway collects data from the MC LoRa end-node devices and are sent to the TTN server. Once the information is received in the TTN server, it is directly forwarded to the Timbercare remote cloud server where it is stored in the database. Lastly, Timbercare application works with the database for data monitoring and management. Due to the low latency times, this infrastructure allows to have data ready in Timbercare immediately after being generated in the MC LoRa end-nodes.

Fig. 16 shows the architecture of the platform developed in the cloud server, composed of three main parts: visual user interface, background processing end-module, and database:

1) User Interface. This interface is based on Bootstrap framework and Angular Js, consisting of a set of CSS classes and JavaScript functions that makes the process of front-end development to be modular, providing a responsive design supporting different screen sizes. In order to help users to browse the data received from the MC LoRa end-nodes conveniently, the interface includes a navigation system among the end-nodes assigned to the user, a messaging system to quickly display alarms or MC values out of limits settled by the user, and a graphical content displayed in the form of charts and tables to display historical data. The platform also includes a 'File Export' function to allow users to export data in different formats for further analysis by off-line software tools. An administration level is implemented in order to manage all the users of the platform.
2) Background end-module. This processing module is configured with LAMP (Linux, Apache, MySQL and PHP) software which is the basis of the host web application. The module includes MVC layers and it is based on Laravel framework. This design provides support for a huge number of simultaneous users using low resources. The platform is using the cache and ORM (Object–Relational Mapping) of Laravel framework to design the Model layer supporting data cache and SQL database operations. The user interface part is connected with the back-end part via the View layer.
3) Database. This part is running MySQL database environment to store the data using different tables. It is based on a multi-process architecture which spawns many processes to support multiple users and connections from either the gateways and the visual interface.

The web application database consists of eight main tables: 'Users', 'Roles', 'Devices', 'Networks', 'Datas', 'Notifications', 'Warnings', and 'Emails':

- **Users**. This table stores the information of users registered in Timbercare (Name, email, address, password, etc.).
- **Roles**. The access level of the users (e.g. Administrator, Moderator, ...). The roles used in this work are 'administrator' and 'user'. The administrator can define other roles in the dashboard. The users are attached to their roles via the 'Role_user' pivot table.
- **Devices**. This table stores the user devices including their identifiers.
- **Networks**. This table registers the LoRa network.
- **Datas**. This table stores the data received from each sensor connected to the LoRa network. The sensors are linked to their data via the 'Device_data' table.
- **Notifications**. This table stores the multiple notifications generated by the platform.
- **Warnings**. When the platform receives a value out of range (defined by the user) from a MC LoRa end-device, a warning message will be generated, stored in this table and sent to the user (the owner of the device).
- **Emails**. The user can define multiple email addresses where warnings and notifications related to the sensors are sent.

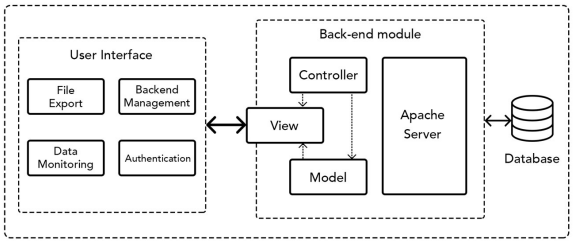

Fig. 16. Timbercare: web monitoring platform architecture for user interface and LoRa data exchange.

The authentication system implemented in the platform protects all data. Only authorized users have access to his specific dashboard according to the MC LoRa end-nodes assigned. Depending on the type of user (administrator or user), it is also possible to add/remove devices, view notifications, monitor the data, and export them. Fig. 17 (a) shows the login fields in the home page and Fig. 17 (b) describes the register page to allow users to create a new account.

The web interface has five main menus: 'Dashboard', 'Device', 'Network', 'Notifications' and 'Profile'.

- **Dashboard**. After the user login to the account, the 'Dashboard' page is shown (Fig. 17 (b)) where the the main view of the associated devices in the network is displayed (both gateways and end-nodes). To view the data charts of a device, the user can click on the device name and is redirected to the 'Device' page.
- **Device**. The device page shows information of an specific MC LoRa end-node and displays the received data in the form of charts. The user can filter the data by defining a time range and export data in the form of CSV or EXCEL files. In this page (Fig. 17 (d)) it is also possible to add new devices: gateways and end-nodes, being able to edit, delete, activate or deactivate a device. The user can set the measurement limits for the sensor nodes. When the sensed value is out of the defined range, the platform generates an alert message shown in the platform and

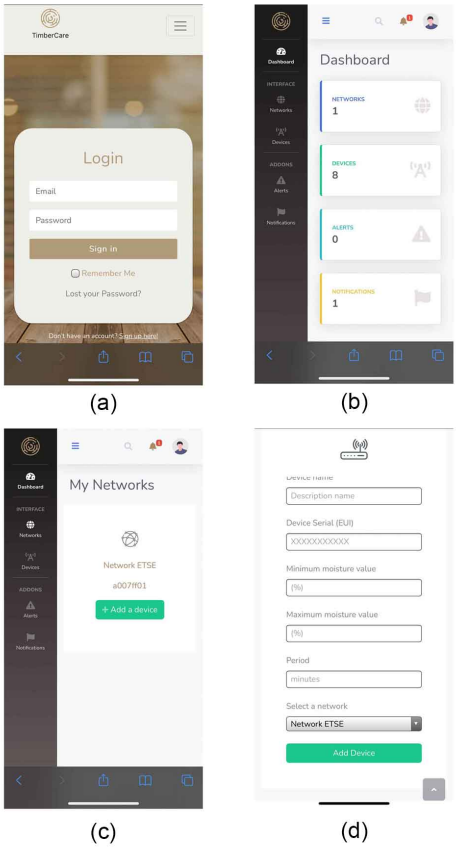

Fig. 17. Screenshots from the Timbercare monitoring and management platform for MC. (a) Home page with login fields, (b) user dashboard page, (c) network settings page, and (d) Register new device screens.

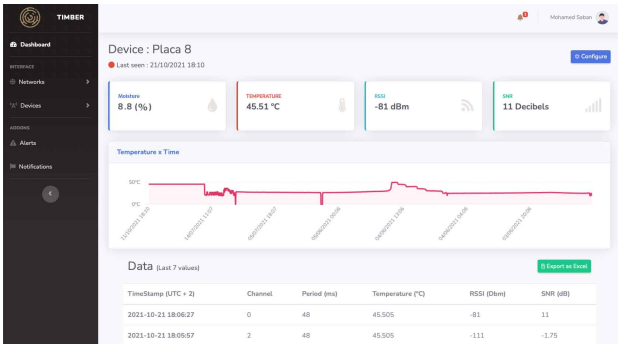

Fig. 18. Screenshots of the device page showing the latest received information from a LoRa end-node device. The user can visualize the temperature and moisture in the form of charts and also can download the data as an excel table.

also sent to the user via email.

- **Network**. This page (Fig. 17 (c)) allows users to add new LoRa networks or update the information of a network. Each device added to the platform must belong to a network.
- **Notifications and Alerts**. The user can check all the messages generated by the platform. In addition to messages related to out of range MC measured values, other messages related to lost connections with end-nodes or gateways can also be displayed. Two classes of messages are defined: 'notifications' and 'alerts' depending on the priority level.
- **Profile**. Profile update of user information is done in this page: avatar, email, password, etc.

Concerning the resource usage of the server, Fig. 19 shows the test results of user operations in the platform. It displays the CPU consumption, the memory usage and the downloaded data size when the system receives user requests. The average response time, as this figure shows, is 125 ms. These results show that the CPU usage slightly increases after receiving a user request and then decreases. In any case, the CPU usage remains low and stable even in multiple concurrent requests, which reflects the high performance and optimization of Timbercare web application. The occupied memory remains lower than 200 Mb in all cases. All the pictures and icons used in the platform use vectorial SVG files, which increases the speed of the platform and consumes low resources. Thus, the size of the downloaded data from the server is not exceeding 2.5 Mb for each request from the user, as seen in the figure.

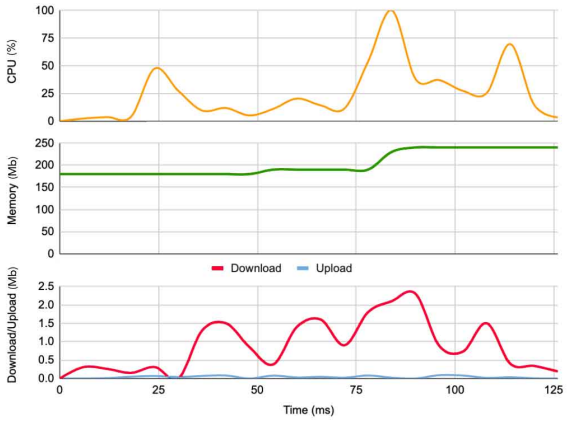

Fig. 19. CPU usage, allocated memory and download/upload of data as a function of time during multiple user interface visualization requests.

VII. Conclusion

This paper describes the development of a complete IoT system for monitoring the moisture content of wood, aimed as a support tool for building maintenance services, especially those based on timber. The proposed infrastructure covers from the sensing end-nodes to the web user interface, based on LoRa and LoRaWan wireless protocols. Electronic boards for MC LoRa end-nodes was completely designed from scratch, obtaining a battery operated electronic board including a novel AC-based measurement method based in an relaxation oscillator which automatically tunes its frequency depending on the resistance of wood, which is reflected in a direct correlation with moisture content.An accuracy lower than 2 % has been achieved in the measurement of wood resistance which is equivalent to an error lower than 0.2 % in the wood MC. The experimental results shows that the developed MC LoRa end-device is accurate and can work in temperature range between 0 °C and 50 °C using different types of wood. Also, the device shows stable measurements during long periods of time.

The device can transmit the data up to 430 meters, and the indoor environment test shows that the LoRa signal covers a 3 floors building in all locations. The end-node on-board microcontroller is programmed to wake up the device, power up the MC sensing circuitry, take the average of three measurement values and send the value to the gateway. Then, the device enters in a sleep mode until the next measure time. This period is chosen by the user in the Timbercare web interface. This mode of operation reduces the power consumption of the device and allows extensive duration of battery.

The open source architecture of LoRaWan allows the connection of the developed devices to the LoRaWan network directly if there is a nearby LoRa gateway, which lowers the cost of installation of this system. Instead, a proprietary LoRa gateway can also be used, as in this work.

The developed web application allows the users to manage their devices, monitor and analyse the collected data. The MVC design pattern helps modify and update the platform easily, thus, the development of the platform is scalable, with more utilities added depending on the users need. This point is very advantageous when deploying the system in different buildings, under different requirements from the final users.

The platform is consuming low server resources, and consequently, a large number of sensor nodes and gateways can be supported, which also means that a large number of concurrent users can use the platform. In any case, the number of simultaneous users depends on the server resources (CPU, storage and RAM memory). The developed platform respects the user experience (UX) and the interface design (UI) is eye-catching, well organized and responsive for all screen sizes.

The system can be used in wooden houses or in heritage buildings such as churches, palaces, or any other timber-based buildings where many structures and furniture needs to be adequately conserved to avoid deterioration.

To conclude, the proposed infrastructure resolves an important need in monitoring an essential parameter as moisture content for timber-based buildings. Additionally, due to its modular and scalable design, it can be extended to more types of nodes (not only sensing MC) to provide integral data sensing in buildings. Moreover, the modular design of the web interface can extend the visualization to multiple users, buildings, and end-nodes, as well as integrate data analysis tools due to the automatic data exchange. Currently, an Artificial Intelligence (AI) data analysis tools is under development.

ACKNOWLEDGMENT

The authors would like to thank the administrator of La Nau historical building and heritage library for their collaboration and interest in this work.

REFERENCES

[1] W. L. James, *Dielectric properties of wood and hardboard: variation with temperature, frequency, moisture content, and grain orientation*. Department of Agriculture, Forest Service, Forest Products Laboratory, 1975, vol. 245.

[2] G. T. Kirker, A. B. Bishell, and S. L. Zelinka, "Electrical properties of wood colonized by gloeophyllum trabeum," *International Biodeterioration & Biodegradation*, vol. 114, pp. 110–115, 2016.

[3] R. R. N. Mvondo, P. Meukam, J. Jeong, D. D. S. Meneses, and E. G. Nkeng, "Influence of water content on the mechanical and chemical properties of tropical wood species," *Results in Physics*, vol. 7, pp. 2096–2103, 2017.

[4] R. J. Ross *et al.*, "Wood handbook: wood as an engineering material. usda forest service, forest products laboratory," *General Technical Report FPL-GTR-190*, vol. 509, no. 5, 2010.

[5] O. Schmidt, *Wood and tree fungi*. Springer, 2006.

[6] K. Patil and N. Kale, "A model for smart agriculture using iot," in *2016 International Conference on Global Trends in Signal Processing, Information Computing and Communication (ICGTSPICC)*. IEEE, 2016, pp. 543–545.

[7] X. Silvani, F. Morandini, E. Innocenti, and S. Peres, "Evaluation of a wireless sensor network with low cost and low energy consumption for fire detection and monitoring," *Fire Technology*, vol. 51, no. 4, pp. 971–993, 2015.

[8] S. S. Siddula, P. Babu, and P. Jain, "Water level monitoring and management of dams using iot," in *2018 3rd International Conference on Internet of Things: Smart Innovation and Usages (IoT-SIU)*. IEEE, 2018, pp. 1–5.

[9] T. Torfs, T. Sterken, S. Brebels, J. Santana, R. van den Hoven, V. Spiering, N. Bertsch, D. Trapani, and D. Zonta, "Low power wireless sensor network for building monitoring," *IEEE Sensors Journal*, vol. 13, no. 3, pp. 909–915, 2012.

[10] J.-Y. Kim, C.-H. Chu, and S.-M. Shin, "Issaq: An integrated sensing systems for real-time indoor air quality monitoring," *IEEE Sensors Journal*, vol. 14, no. 12, pp. 4230–4244, 2014.

[11] U. Raza, P. Kulkarni, and M. Sooriyabandara, "Low power wide area networks: An overview," *IEEE Communications Surveys & Tutorials*, vol. 19, no. 2, pp. 855–873, 2017.

[12] A. Al-Fuqaha, M. Guizani, M. Mohammadi, M. Aledhari, and M. Ayyash, "Internet of things: A survey on enabling technologies, protocols, and applications," *IEEE communications surveys & tutorials*, vol. 17, no. 4, pp. 2347–2376, 2015.

[13] A. Whitmore, A. Agarwal, and L. Da Xu, "The internet of things—a survey of topics and trends," *Information systems frontiers*, vol. 17, no. 2, pp. 261–274, 2015.

[14] A. Wasicek, "The future of 5g smart home network security is micro-segmentation," *Network Security*, vol. 2020, no. 11, pp. 11–13, 2020. [Online]. Available: https://www.sciencedirect.com/science/article/pii/S135348582030129X

[15] D. Hardilla and A. C. Nugroho, "The role of internet of things to support cultural heritage inventory in urban resiliency approach: Tradisional house in bandar lampung case," in *2018 International Conference on Information Technology Systems and Innovation (ICITSI)*. IEEE, 2018, pp. 193–198.

[16] D. R. Gawade, S. Ziemann, S. Kumar, D. Iacopino, M. Belcastro, D. Alfieri, K. Schuhmann, M. Anders, M. Pigeon, J. Barton, *et al.*, "A smart archive box for museum artifact monitoring using battery-less temperature and humidity sensing," *Sensors*, vol. 21, no. 14, p. 4903, 2021.

[17] A. Marra, S. Gerbino, A. Greco, and G. Fabbrocino, "Combining integrated informative system and historical digital twin for maintenance and preservation of artistic assets," *Sensors*, vol. 21, no. 17, p. 5956, 2021.

[18] L. J. Klein, S. A. Bermudez, A. G. Schrott, M. Tsukada, P. Dionisi-Vici, L. Kargere, F. Marianno, H. F. Hamann, V. López, and M. Leona, "Wireless sensor platform for cultural heritage monitoring and modeling system," *Sensors*, vol. 17, no. 9, p. 1998, 2017.

[19] M. Gribaudo, M. Iacono, and A. H. Levis, "An iot-based monitoring approach for cultural heritage sites: The matera case," *Concurrency and Computation: Practice and Experience*, vol. 29, no. 11, p. e4153, 2017.

[20] M. Maksimović and M. Ćosović, "Preservation of cultural heritage sites using iot," in *2019 18th International Symposium INFOTEH-JAHORINA (INFOTEH)*. IEEE, 2019, pp. 1–4.

[21] F. Colace, C. Elia, C. G. Guida, A. Lorusso, F. Marongiu, and D. Santaniello, "An iot-based framework to protect cultural heritage buildings," in *2021 IEEE International Conference on Smart Computing (SMARTCOMP)*. IEEE, 2021, pp. 377–382.

[22] F. Piccialli, P. Benedusi, L. Carratore, and G. Colecchia, "An iot data analytics approach for cultural heritage," *Personal and Ubiquitous Computing*, pp. 1–8, 2020.

[23] L. Alliance *et al.*, "Lorawan what is it," *A technical overview of LoRa and LoRaWAN*, pp. 5–17, 2015.

[24] H. A. Al-Kashoash and A. H. Kemp, "Comparison of 6lowpan and

lpwan for the internet of things," *Australian Journal of Electrical and Electronics Engineering*, vol. 13, no. 4, pp. 268–274, 2016.

[25] L. Carosso, L. Mattiauda, and M. Allegretti, "A survey on devices exploiting lora communication." *Acta Marisiensis. Seria Technologica.*, vol. 17, no. 2, 2020.

[26] W. Guibene, J. Nowack, N. Chalikias, K. Fitzgibbon, M. Kelly, and D. Prendergast, "Evaluation of lpwan technologies for smart cities: River monitoring use-case," in *2017 IEEE Wireless Communications and Networking Conference Workshops (WCNCW)*. IEEE, 2017, pp. 1–5.

[27] A. Augustin, J. Yi, T. Clausen, and W. M. Townsley, "A study of lora: Long range & low power networks for the internet of things," *Sensors*, vol. 16, no. 9, p. 1466, 2016.

[28] J. Haxhibeqiri, A. Karaagac, F. Van den Abeele, W. Joseph, I. Moerman, and J. Hoebeke, "Lora indoor coverage and performance in an industrial environment: Case study," in *2017 22nd IEEE international conference on emerging technologies and factory automation (ETFA)*. IEEE, 2017, pp. 1–8.

[29] L. Specification, "v1. 1 available at: https://loraalliance. org/resource-hub/lorawantm-specification-v11," *Online Accessed*, vol. 10, 2018.

[30] L. Alliance, "A technical overview of lora and lorawan," *white paper, November*, vol. 20, 2015.

[31] IMST, "im881a-xl lora® radio module - wireless solutions application," Mar 2021. [Online]. Available: https://wireless-solutions.de/products/lora-solutions-by-imst/radio-modules/im881a-xl/

[32] P. Dietsch, S. Franke, B. Franke, A. Gamper, and S. Winter, "Methods to determine wood moisture content and their applicability in monitoring concepts," *Journal of Civil Structural Health Monitoring*, vol. 5, no. 2, pp. 115–127, 2015.

[33] A. J. Stamm, "The electrical resistance of wood as ameasure of its moisture content," *Industrial & Engineering Chemistry*, vol. 19, no. 9, pp. 1021–1025, 1927.

[34] S. Casans, T. Iakymchuk, and A. Rosado-Muñoz, "High resistance measurement circuit for fiber materials: Application to moisture content estimation," *measurement*, vol. 119, pp. 167–174, 2018.

[35] C. Moron, L. Garcia-Fuentevilla, A. Garcia, and A. Moron, "Measurement of moisture in wood for application on rehabilitation of old buildings," in *2nd International Electronic Conference on Sensors and Applications*. Multidisciplinary Digital Publishing Institute, 2015.

[36] J. Wang, P. Mukhopadhyaya, and P. I. Morris, "Sorption and capillary condensation in wood and the moisture content of red pine," *Journal of Building Physics*, vol. 37, no. 4, pp. 327–347, 2014.

[37] J. Johansson, O. Hagman, and B.-A. Fjellner, "Predicting moisture content and density distribution of scots pine by microwave scanning of sawn timber," *Journal of Wood Science*, vol. 49, no. 4, pp. 312–316, 2003.

[38] V. Tamme, P. Muiste, and H. Tamme, "Experimental study of resistance type wood moisture sensors for monitoring wood drying process above fibre saturation point/takistus-tüüpi puidu niiskuse andurite eksperimentaalne uurimine puidu kuivatamise monitooringul niiskussisaldustel üle kiu küllastuspunkti," *Forestry Studies/Metsanduslikud Uurimused*, vol. 59, no. 1, 2013.

[39] S. Casans Berga, R. Garcia-Gil, A. E. Navarro Anton, and A. Rosado-Muñoz, "Novel wood resistance measurement method reducing the initial transient instabilities arising in dc methods due to polarization effects," *Electronics*, vol. 8, no. 11, p. 1253, 2019.

[40] G. Dai and K. Ahmet, "Long-term monitoring of timber moisture content below the fiber saturation point using wood resistance sensors," *Forest Products Journal*, vol. 51, no. 5, p. 52, 2001.

[41] S. Gao, Z. Bao, L. Wang, and X. Yue, "Comparison of voltammetry and digital bridge methods for electrical resistance measurements in wood," *Computers and Electronics in Agriculture*, vol. 145, pp. 161–168, 2018.

[42] A. Samuelson, *Resistanksurvor für elektriska fuktkvotsmätare. TräteknikCentrum*. Rapport L 9006029, Stockholm, 37pp, 1990.

[43] H. Forsén, V. Tarvainen, *et al.*, *Accuracy and functionality of hand held wood moisture content meters*. Technical Research Centre of Finland Espoo,, Finland, 2000.

[44] J. F. Golfin, M. C. García, R. M. C. Haro, M. B. Merino, and P. de Palacios, "Curves for the estimation of the moisture content of ten hardwoods by means of electrical resistance measurements," *Forest Systems*, vol. 21, no. 1, pp. 121–127, 2012.

[45] A. Hambley, *Electronics*. Prentice Hall, 2000. [Online]. Available: https://books.google.es/books?id=0et7QgAACAAJ

[46] A. Sedra and K. Smith, *Microelectronic Circuits*, ser. Oxford series in electrical and computer engineering. Oxford University Press, 2004. [Online]. Available: https://books.google.es/books?id=9UujQgAACAAJ

[47] P. Garrahan, "Moisture meter correction factors. forintek canada corp," in *Proceedings of a seminar on "In-grade testing of structural lumber", held at uSDA Forest Products laboratory, Madison WI*, 1988.

[48] D. M. Onysko, C. Schumacher, and P. Garrahan, "Field measurements of moisture in building materials and assemblies: pitfalls and error assessment," in *Best 1 Conference–Building Enclosure Science & Technology*, 2008.

[49] N. Blenn and F. Kuipers, "Lorawan in the wild: Measurements from the things network," *arXiv preprint arXiv:1706.03086*, 2017.

[50] J. Petajajarvi, K. Mikhaylov, A. Roivainen, T. Hanninen, and M. Pettissalo, "On the coverage of lpwans: range evaluation and channel attenuation model for lora technology," in *2015 14th international conference on its telecommunications (itst)*. IEEE, 2015, pp. 55–59.

[51] J. Gaelens, P. Van Torre, J. Verhaevert, and H. Rogier, "Lora mobile-to-base-station channel characterization in the antarctic," *Sensors*, vol. 17, no. 8, p. 1903, 2017.

[52] M. Cattani, C. A. Boano, and K. Römer, "An experimental evaluation of the reliability of lora long-range low-power wireless communication," *Journal of Sensor and Actuator Networks*, vol. 6, no. 2, p. 7, 2017.

[53] P. Neumann, J. Montavont, and T. Noel, "Indoor deployment of low-power wide area networks (lpwan): A lorawan case study," in *2016 IEEE 12th International Conference on Wireless and Mobile Computing, Networking and Communications (WiMob)*. IEEE, 2016, pp. 1–8.

[54] S. Benaissa, D. Plets, E. Tanghe, J. Trogh, L. Martens, L. Vandaele, L. Verloock, F. Tuyttens, B. Sonck, and W. Joseph, "Internet of animals: characterisation of lora sub-ghz off-body wireless channel in dairy barns," *Electronics Letters*, vol. 53, no. 18, pp. 1281–1283, 2017.

[55] P. A. Barro, M. Zennaro, and E. Pietrosemoli, "Tltn–the local things network: on the design of a lorawan gateway with autonomous servers for disconnected communities," in *2019 Wireless Days (WD)*. IEEE, 2019, pp. 1–4.

[56] T. Ameloot, P. Van Torre, and H. Rogier, "Indoor body-to-body lora link characterization," in *2019 IEEE-APS Topical Conference on Antennas and Propagation in Wireless Communications (APWC)*. IEEE, 2019, pp. 042–047.

[57] P. Wojcicki, T. Zientarski, M. Charytanowicz, and E. Lukasik, "Estimation of the path-loss exponent by bayesian filtering method," *Sensors*, vol. 21, no. 6, p. 1934, 2021.

[58] T. S. Rappaport *et al.*, *Wireless communications: principles and practice*. prentice hall PTR New Jersey, 1996, vol. 2.

[59] G. M. Bianco, R. Giuliano, G. Marrocco, F. Mazzenga, and A. Mejia-Aguilar, "Lora system for search and rescue: Path-loss models and procedures in mountain scenarios," *IEEE Internet of Things Journal*, vol. 8, no. 3, pp. 1985–1999, 2020.

[60] "La nau." [Online]. Available: https://www.uv.es/uvweb/culture/en/la-nau/la-nau-cultural-centre/presentation-1285866274374.html

[61] S. Y. Seidel and T. S. Rappaport, "914 mhz path loss prediction models for indoor wireless communications in multifloored buildings," *IEEE transactions on Antennas and Propagation*, vol. 40, no. 2, pp. 207–217, 1992.

[62] W. Xu, J. Y. Kim, W. Huang, S. S. Kanhere, S. K. Jha, and W. Hu, "Measurement, characterization, and modeling of lora technology in multifloor buildings," *IEEE Internet of Things Journal*, vol. 7, no. 1, pp. 298–310, 2019.

[63] R. F. Olanrewaju, T. Islam, and N. Ali, "An empirical study of the evolution of php mvc framework," in *Advanced Computer and Communication Engineering Technology*. Springer, 2015, pp. 399–410.

MOHAMED SABAN received his Master Degree in Networks and Telecommunications Engineering in 2017, from the National School of Applied Sciences of Tetouan (ENSAT), University of Abdelmalek Essaâdi, Morocco. Currently, he is working towards his PhD in Electronic Engineering at the engineering school ETSE, University of Valencia, Spain. His research interests include wireless sensor networks, IoT networks, development of new IoT sensors and development of IoT monitoring applications.

SILVIA CASANS BERGA received the M.Sc. degree in physics and the Ph.D. degree in electronics from the University of Valencia, Valencia, Spain, in 1999 and 2002, respectively. She is currently with the Department of Electronic Engineering, University of Valencia. Her research interests include electronic instrumentation and sensors and their instrumentation systems.

RAFAEL GARCÍA-GIL received the M.Sc. degree in physics, the second M.Sc. degree in electronic engineering, and the Ph.D. degree in electronics from the University of Valencia, Spain, in 1993, 1995, and 2002, respectively. Since 1998, he has been with the Electronics Engineering Department, University of Valencia, where he is currently an Associate Professor. His main research interests include power converters for renewable energy applications, sensor characterization, and electronic instrumentation.

EDITH NAVARRO ANTÓN received the M.Sc. degree in physics and the Ph.D. degree in electronics from the University of Valencia, Valencia, Spain in 1992 and 1997, respectively. She is currently an Associate Professor with the Department of Electronic Engineering, University of Valencia, where she is teaching microelectronics and IC technology. Her research interests include the design of distributed measurement systems and industrial projects related to electronic instrumentation.

OTMAN AGHZOUT received the Ph.D. degree in telecommunications engineering from the High School of Telecommunications Engineering, University of Las Palmas de Gran Canaria, Spain, in January 2002. He was a Researcher Student with the Microwave Group, Department of Electronics and Electromagnetism, University of Seville, Spain, from 1996 to 1999. In January 2002, he joined the Medical Technology Center, University Hospital of GC, where he worked in medical engineering applications, for a period of two years, from 2002 to 2004. He is participant of NA-MIC Projects, Hospital y Brigham Women's of the the University of Harvard. In 2009, he joined the National School of Applied Sciences, Abdelmalek Essaadi University, Tetouan, Morocco. He is currently a full Professor with the Department of Computer Science Engineering. His research interests include printed microwave passive and active circuits, filters, antenna designs, medical imaging systems, theory of characteristic modes analysis, the Internet of Things, and smart cities applications.

ALFREDO ROSADO-MUÑOZ received the M.Sc. and Ph.D. degrees in physics from the Universitat de Valencia, Spain, in 1994 and 2000, respectively. He is a member of the International Federation of Automatic Control. He is currently a Professor with the Department of Electronic Engineering, Universitat de Valencia. His work is related to digital hardware design (embedded systems) for digital signal processing, artificial intelligence and control systems, especially targeted for biomedical engineering, and bio-inspired systems. He also works on neuromorphic hardware and automation systems.